



Protein kinase C-mediated phosphorylation of transient receptor potential melastatin type 2 Thr738 counteracts the effect of cytosolic Ca²⁺ and elevates the temperature threshold

Makiko Kashio¹ , Satoru Masubuchi² and Makoto Tominaga^{1,3} 

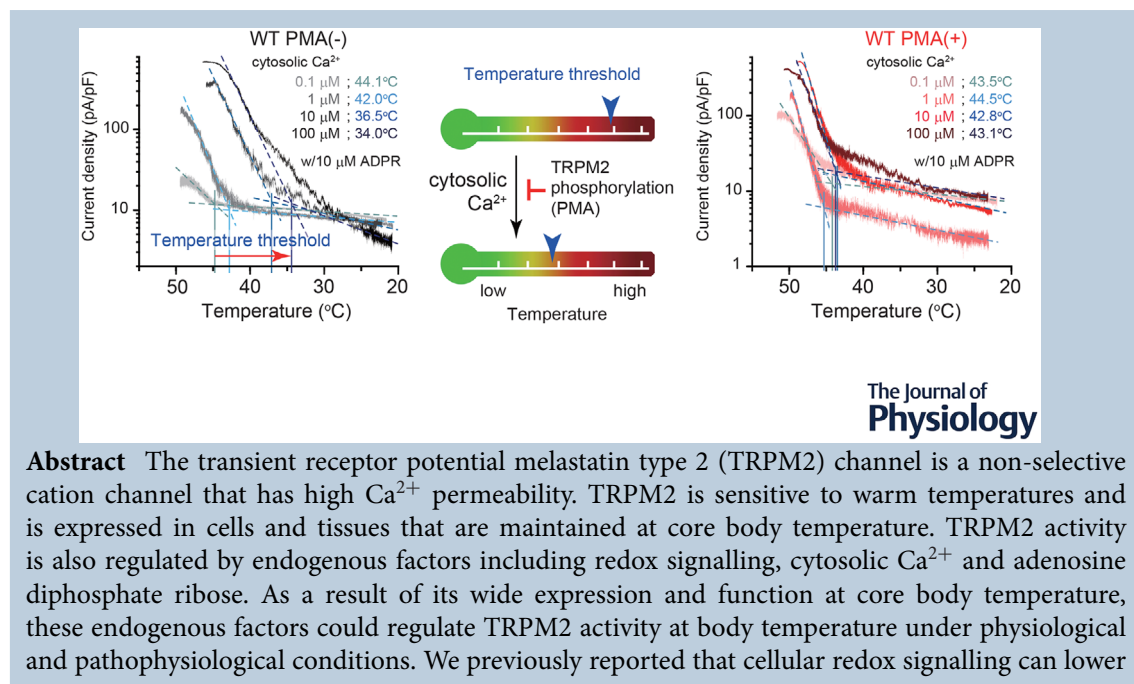
¹Division of Cell Signaling, National Institute for Physiological Sciences, National Institutes for Natural Sciences, Okazaki, Aichi, Japan

²Department of Physiology, Aichi Medical University, Nagakute, Aichi, Japan

³Thermal Biology Group, Exploratory Research Center on Life and Living Systems (ExCELLS), National Institutes of Natural Sciences, Okazaki, Aichi, Japan

Handling Editors: David Wyllie & Carole Torsney

The peer review history is available in the Supporting information section of this article (<https://doi.org/10.1113/JP283350#support-information-section>).



Makiko Kashio is an Associate Professor in Division of Cell Signaling at National Institute for Physiological Sciences (NIPS). She completed her PhD at the Graduate University for Advanced Studies (SOKENDAI), followed by a postdoctoral position in the Division of Cell Signaling at NIPS, an assistant professorship in the Department of Molecular Cell Physiology at Kyoto Prefectural University of Medicine, and a lectureship in the Department of Physiology at Aichi Medical University. Her main areas of interest are the regulatory mechanisms of thermo-sensitive TRP channels and their physiological roles under the body temperature.



TRPM2 temperature thresholds, although the mechanism that regulates these thresholds is unclear. Here, we used biochemical and electrophysiological techniques to explore another regulatory mechanism for TRPM2 temperature thresholds that is mediated by TRPM2 phosphorylation. Our results show that: (1) the temperature threshold for TRPM2 activation is lowered by cytosolic Ca^{2+} ; (2) protein kinase C-mediated phosphorylation of TRPM2 counteracts the effect of cytosolic Ca^{2+} ; and (3) Thr738 in mouse TRPM2 that lies near the Ca^{2+} binding site in the cytosolic cleft of the transmembrane domain is a potential phosphorylation site that may be involved in phosphorylation-mediated elevation of TRPM2 thresholds. These findings provide structure-based evidence to understand how temperature thresholds of thermo-sensitive TRP channels (thermo-TRPs) are determined and regulated.

(Received 20 May 2022; accepted after revision 26 August 2022; first published online 30 August 2022)

Corresponding author M. Kashio: Division of Cell Signaling, National Institute for Physiological Sciences, National Institutes for Natural Sciences, Okazaki, Aichi, 444–8787, Japan. Email: mkashio@nips.ac.jp

Abstract figure legend The transient receptor potential melastatin type 2 (TRPM2) ion channel is Ca^{2+} -permeable and has temperature sensitivity in the body temperature range. Endogenous factors and pathways such as redox signalling can regulate TRPM2 activity at body temperature under physiological and pathophysiological conditions. We report the novel finding that cytosolic Ca^{2+} lowers the temperature threshold for TRPM2 activation in a concentration-dependent manner. Protein kinase C-mediated phosphorylation of TRPM2 elevates the threshold by counteracting the effects of cytosolic Ca^{2+} . Thr738 in mouse TRPM2 lies near the Ca^{2+} binding site in the cytosolic cleft of the transmembrane domain and is a potential phosphorylation site that may be involved in phosphorylation-mediated elevation of TRPM2 thresholds. These findings provide structure-based evidence to understand how temperature thresholds of thermo-sensitive TRP channels are determined and regulated.

Key points

- The transient receptor potential melastatin type 2 (TRPM2) ion channel is temperature-sensitive and Ca^{2+} -permeable.
- Endogenous factors and pathways such as redox signalling can regulate TRPM2 activity at body temperature under physiological and pathophysiological conditions.
- In the present study, we report the novel finding that cytosolic Ca^{2+} lowers the temperature threshold for TRPM2 activation in a concentration-dependent manner.
- Protein kinase C-mediated phosphorylation of TRPM2 at amino acid Thr782 elevates the temperature threshold for activation by counteracting the effects of cytosolic Ca^{2+} .
- These findings provide structure-based evidence to understand how temperature thresholds of thermo-sensitive TRP channels are determined and regulated.

Introduction

The transient receptor potential (TRP) channel super family in mammals is composed of multiple sub-families: canonical (C), vanilloid (V), melastatin (M), polycystin (P), mucolipin (ML) and ankyrin (A) (Ramsey et al., 2006). As a shared structure of TRP channels, the functional channel is formed by a tetramer of subunits each having six transmembrane (TM) segments (S1–6), a pore domain between S5 and S6, and cytosolic amino and carboxyl termini. Many TRP channels are non-selective cation channels that have high Ca^{2+} permeability. Activation of these channels causes membrane depolarisation and intracellular Ca^{2+} elevation that regulates cell excitability

and intracellular processes, respectively. TRP channels have characteristic effective stimuli, such as chemical compounds and mechanical stimuli (Ramsey et al., 2006). Several TRP channels activated by temperature changes are called thermo-sensitive TRP channels (thermo-TRPs) (Kashio & Tominaga, 2022). Subsequent to the discovery of temperature-dependent activation of TRPV1, a founding member of mammalian thermo-TRPs, other thermo-TRPs have been characterised according to their temperature sensitivity (Caterina et al., 1997). To date, TRPV1–4, TRPA1, TRPC5, TRPM2–5 and TRPM8 have been reported to be thermo-TRPs (Kashio & Tominaga, 2022). Each of these thermo-TRPs has a characteristic temperature threshold, and they are activated at a wide range of ambient and physiological temperatures.

However, the thresholds for these thermo-TRPs are not necessarily fixed.

One mechanism for modulation of temperature thresholds involves synergistic effects between temperature and other effective stimuli. TRPV1 is a heat sensor that detects noxious heat in peripheral sensory neurons to cause painful sensations and defensive behaviours. Effective activators, such as capsaicin and protons, decrease the temperature thresholds for TRPV1 activation (Tominaga et al., 1998). TRPM8 is a cool temperature sensor in sensory neurons, and its activation causes comfortable cool sensations. Temperature thresholds for TRPM8 are synergistically increased by the activator menthol to enhance cool sensations (McKemy et al., 2002). Post-translational modifications are also reported to regulate temperature thresholds for some thermo-TRPs. Phosphorylation of TRPV1 by protein kinase C (PKC) or protein kinase A (PKA) is known to decrease temperature thresholds or increase responsiveness of heat-evoked TRPV1 activity (Moriyama et al., 2005; Numazaki et al., 2002; Rathee et al., 2002; Vellani et al., 2001). Such reductions in TRPV1 thresholds can cause activation at body temperature and hyperalgesia that is induced by algescic inflammatory mediators including ATP and prostaglandin E2 (Moriyama et al., 2005; Numazaki et al., 2002). Despite the physiological and clinical significance of thermo-TRPs, the detailed mechanisms by which the temperature thresholds of these channels are modulated have not been fully characterised.

TRPM2 is another thermo-TRP that functions as a non-selective cation channel with high Ca^{2+} permeability that induces increases in intracellular Ca^{2+} concentrations modifying many cellular processes (Sumoza-Toledo & Penner, 2011). TRPM2 is broadly expressed in hematopoietic lineage cells, as well as in the pancreas, brain, and sensory and autonomic neurons. It plays roles in cell death, immune responses, insulin secretion, warmth sensation and body temperature regulation (Kamm et al., 2021; Song et al., 2016; Sumoza-Toledo & Penner, 2011; Tan et al., 2016; Togashi et al., 2006; Uchida et al., 2011). In addition to temperature, TRPM2 activity is reportedly regulated by several endogenous factors including redox signalling, cytosolic Ca^{2+} and adenosine diphosphate ribose (ADPR) (Kashio & Tominaga, 2017). Based on its broad expression and function at core body temperature, TRPM2 activity at body temperature is considered to be effectively regulated by the above-mentioned endogenous factors under physiological and pathophysiological conditions. As a result of this functional regulation, TRPM2 is considered to act as a body temperature sensor.

We previously reported that the temperature threshold for naïve TRPM2 channels in the absence of endogenous activators is around 47°C , and that this threshold can be lowered to the physiological temperature range

(< 37°C) through methionine oxidation mediated by hydrogen peroxide (H_2O_2), a functional molecule involved in redox signalling (Kashio et al., 2012). H_2O_2 is considered to modulate TRPM2 thresholds and elevated TRPM2 activity at body temperature could promote its physiological function. Similar to TRPV1, however, the detailed mechanisms involved in regulating temperature thresholds for TRPM2 activation have not been explored. The present study aimed to discover other regulatory mechanisms of temperature thresholds for TRPM2 activation, with a focus on TRPM2 phosphorylation.

Methods

Cell culture

Human embryonic kidney-derived 293T (HEK293T) cells (RIKEN BRC, Ibaraki, Japan) were cultured in Dulbecco's Eagle's medium (Wako Pure Chemical Industries, Osaka, Japan) containing penicillin/streptomycin (Thermo Fisher Scientific, Waltham, MA, USA) and 10% heat-inactivated fetal bovine serum (Thermo Fisher Scientific) at 37°C in a humidified 5% CO_2 incubator.

Construction of expression vectors

Mouse TRPM2 cDNAs in the pCIneo expression vector were generously provided by Dr Mori (Kyoto Univ., Kyoto, Japan). Mouse TRPM2 or hemagglutinin (HA)-tagged mouse TRPM2 cDNAs were cloned into pcDNA3.1(+) by PCR-based cloning. Vectors containing the full-length mutants were constructed by single amino acid substitutions using a modified QuikChange Site-Directed Mutagenesis method (Agilent Technologies, Inc., Santa Clara, CA, USA). Candidate Ser/Thr residues involved in phosphorylation by PKC were predicted by NetPhos-3.1 (<https://services.healthtech.dtu.dk/service.php?NetPhos-3.1>). Synthetic oligonucleotide primers containing specific mutations are shown in Table 1. Expression vectors containing alanine mutations in full-length TRPM2 cDNA were reconstructed in the pcDNA3.1(+) expression vector. The entire sequence including the desired alanine substitutions in the mutants was confirmed by DNA sequencing.

Biochemical experiments

HEK293T cells were seeded at 7×10^4 or 3×10^4 cells/well in 24-well plates 24 and 48 h before transfection, respectively. Expression vectors containing HA-tagged TRPM2 cDNAs ($0.2 \mu\text{g}$) were transfected to cells using Lipofectamine 3000 (Invitrogen, Carlsbad, CA, USA). At 20–24 h after transfection, the cells were treated with culture medium containing phorbol myristate acetate

Table 1. PCR primers used to produce site-directed mutations (shown in lower case)

Mutation	Sense primers (5'- to 3')	Antisense primers (5'- to 3')
S21A	GAGGAGGGCTTTGGGGTGCAgCAAGGAGG	CCCAGGTCAGTGGCCCTCTTgCtGCACC
S39A	CCGACGAAGCAATAGCgcCCTTTGCAAGAGCAGG	CCTGCTTGGCAAAGGgcGCTATTGCTTCGTCGG
S49A	GCAGGAGATTCTGTGcGcCTTTAGCAGTGAGAAG	CTTCTACTGCTGAAAGcGCACAGAAATCTCCTGC
S52A	AGATTTCTGTGCTCTTTAGCgcTGAGAAGCAA GAAAACCTTAG	CTAAGGTTTTCTGCTTCTCAgcGCTGAAAGAGC ACAGAAATCT
S77A	GTGTGTGTAactTCGTGGAAgcTTCCAACTCTCGGACG	CGTCCGAGAGTTTGGAAgcTTCCACGAAGTACACACAC
T106A	CCATCAAGCCACACgCCTTCCAGGGCAAG	CTTGCCCTGGAAGGcGTGTGGCTTGATGG
T132A	TTGGTGACATCGTTTTcGcAGACCTGAGCCAGAA	TTTCTGGCTCAGGTCTGcGAAAACGATGTACCAA
S135A	CATCGTTTTACAGACCTGgcCCAGAAAGTGGGGAAAGTAT	ATACTTCCCCACTTTCTGGgcCAGGTCTGTGAAAACGATG
S151A	CAGGACACGCCCTCCgcTGTATCTACCAGCT	AGCTGGTAGATGACAgcGGAGGGCGTGTCTCTG
T173A	CTCATCTCCGTGgCCGGTGGGGCCA	TGGCCCCACCGgcCAGGGAGATGAG
S187A	GAAGCTGAGGCTGAAGgcCATCTTCCGGAGAGGC-	GCCTCTCCGGAAGATGgcCTTACGCTCAGCTTC
T199A	CAAGGTGGCTCAAgCCACGGGGGC	GGCCCCCGTGGcTTGAGCCACCTTG
S227A	TACGGGACTTCAGTCTGgcCAGCAGCTGCAAAGAAG	CTTCTTTCAGCTGCTGgcCAGACTGAAGTCCCCTGA
S228A	GGGACTTCAGTCTGAGCgcCAGCTGCAAAGAAGGTG	CACCTTCTTTCAGCTGgcGCTCAGACTGAAGTCCC
S229A	GACTTCAGTCTGAGCAGCgcCTGCAAAGAAGGTGAAGT	ACTTACCTTCTTTCAGAgcGCTGCTCAGACTGAAGT
T245A	GCCACGTGGGGCgCCATCCACAACC	GGTTGTGGATGGcGCCCCACGTGGC
T290A	TTGGTGGATGATGGGgCCCACGGGCAATATG	CATATTGCCCGTGGcCCCATCATCCACCAA
T302A	TGGAGATCCGCTGAGGgCTAAGCTGAAAAGTTC	GAACTTTCCAGCTTAGcCCTCAGCGGAATCTCCA
S376A	TCTCTGAGATCACCATCgCCTTGATCCAGCAGAAG	CTTCTGCTGGATCAAGGcGATGGTGTATCTCAGAGA
S383A	CTTGATCCAGCAGAAGCTgcCATATTCTCCAGGAGATG	CATCTCTGGAAGAATATGgcGAGCTTCTGCTGGATCAAG
T402A	GAAAACCAGATTGTGGAATGgGcCAAAAAGATCCAAG ACATTG	CAATGTCTGGATCTTTTGGcCCATTCCACAATCTGGTTTTC
T416A	CGGCAGCTGCTGgCGATCTTCCGGG	CCCGGAAGATCGcCAGCAGCTGCCG
T589A	CACGGCTCTCGATGgCCGTGCCACACATC	GATGTGTGGCACGGcCATCGAGAGCCGTG
S604A	GAGTGAGCCTCCGGgCCCTCTATAAGCGA	TCGCTTATAGAGGGcCCGGAGGCTCACTC
T610A	CCCTCTATAAGCGATCAgCAGGCCACGTTACCTTC	GAAGGTAACGTGGCCTGcTGATCGCTTATAGAGGG
T616A	GGCCACGTTACCTTcGcCATTTGACCCAGTCC	GGACTGGGTCAATGGcGAAGGTAACGTGGCC
T689A	GAGCTATAGCGCTTCTcGcTGAGTGCTACAGGAAG	CTTCTGTAGCACTCAGcGAAGACGCTATAGCTC
T738A	GCATCCAGGCTTCTCTAgCAAGGTGTGGTG	CACCACACCTTGGcTAGGAAAGCCTGGATGC
T738D	CATCCAGGCTTCTCTAgCAAGGTGTGGTGGGGC	GCCCCACCACCTTGTcTAGGAAAGCCTGGATG
S1149A	GCAGAAAATCCAAGACATCgcTGAGAAAAGTGGACACCATG	CATGGTGTCCACTTTCTCAgcGATGTCTTGGATTTCTGC
T1193A	TTTGCCTGGATCGTGGcCAACCTGAAGGACAG	CTGTCTTTCAGGGTGGcCAGATCCAGTGCAAA
T1194A	TTGCACTGGATCGTGACAgCCCTGAAGGAC	CCAAAGCCACTGTCTTTCAGGGcGTGTCAGC
S1223A	GATGAGCCAGATGCTGAGCTGgcTATCAGG	CTCTACTTCTCTGATAgcCAGCTCAGC
T1304A	GTGGATGGACCgCGGACCGTCGCA	TGCGACGGTCCGcCGGTCCATCCAC
S1334A	TGCGTGGTCTGGGGgcCCTCAGCTGGTTTG	CAAACCAGCTGAGGgcCCCACGACCAGCA
S1363A	AGCCATCTGCCGGAAGgcTGTCAGGAAGATGCTG	CAGCATCTTCTGACAgcCTTCCGGCAGATGGCT
T1438A	ATGCCTGGATCGAGgCAGTGGCTGTGACG	GCTGACAGCCACTGcCTCGATCCAGGCAT

(PMA, 100 nM) (Wako Pure Chemical Industries) or forskolin (FK, 10 μ M) (Wako Pure Chemical Industries) for 20 min at 37°C, and were then washed twice with divalent-free phosphate-buffered saline [PBS (–)] to remove the PMA or FK. PBS (–) was replaced with normal culture medium and culture was resumed for the indicated durations.

After the indicated culture period, the cells were washed twice with divalent-free tris-buffered saline [TBS (–)] and protein extracts were prepared using

extraction buffer TBS (–) containing 1% Triton X-100, phenylmethylsulfonyl fluoride (Nacalai Tesque, Inc., Kyoto, Japan), protease inhibitor mixture (Nacalai Tesque) and EDTA-free phosphatase inhibitor (Nacalai Tesque). For phosphatase and glycosidase treatment, protein lysates were treated with lambda protein phosphatase (λ PP; Invitrogen, 30°C for 60 min) and peptide-N-glycosidase F (PNGase F; New England Biolabs, Ipswich, MA, USA, 37°C for 60 min), respectively. Protein extracts were denatured (5% 2-mercaptoethanol, 37°C for 60 min)

and 10 μg protein was used for electrophoresis. Normal SDS-PAGE was carried out using a standard protocol. Phos-tag SDS-PAGE was conducted using PAGE gels containing 20 μM Phos-tag acrylamide AAL (NARD Institute, Ltd., Hyogo, Japan) and 40 μM MnCl_2 . To increase transfer efficiency, Mn^{2+} ions were eliminated by soaking Phos-tag SDS-PAGE gels in transfer buffer containing 1 mM EDTA, and transfer buffer containing 0.1% SDS was used for the transfer step. Immunoblotting was performed using anti-HA (dilution 1:1000; 561, MBL Co. Ltd., Tokyo, Japan) and anti- β -tubulin (dilution 1:2000; NB600-936, Novus Biologicals, LLC, Centennial, CO, USA) antibodies. All the antibodies were dissolved in TBS (–) containing 5% non-fat milk and 0.1% Tween-20. Densitometric measurement of protein bands was performed using ImageJ (National Institutes of Health, Bethesda, MD, USA).

Electrophysiology

HEK293T cells were seeded at densities of 5×10^5 or 2×10^5 cells per 35 mm dish, 24 and 48 h before transfection, respectively. Expression vector (1 μg) carrying mouse TRPM2 [wild-type (WT)] or HA-tagged mouse TRPM2 (mutants) with 0.1 μg pGreen Lantern 1 cDNA was transfected to cells using Lipofectamine 3000 (Invitrogen). Successfully transfected cells were identified by green fluorescence and used for experiments 20–36 h after transfection. Whole-cell patch clamp recording was conducted using a standard bath solution containing 140 mM NaCl, 5 mM KCl, 2 mM MgCl_2 , 2 mM CaCl_2 , 10 mM Hepes and 10 mM glucose at pH 7.4 adjusted with NaOH. The pipette solution contained 140 mM CsCl, 5 mM EGTA and 10 mM Hepes at pH 7.4 adjusted with CsOH. Bath solution used in the extracellular Ca^{2+} -free condition was prepared by adding 5 mM EGTA instead of 2 mM CaCl_2 to the standard bath solution. For recording with a series of cytosolic free- Ca^{2+} concentrations, the CaCl_2 concentration was calculated using Maxchelator software (<https://somapp.ucdmc.ucdavis.edu/pharmacology/bbers/maxchelator/CaEGTA-TS.htm>) and was added to the pipette solution with 5 mM EGTA to achieve each concentration of free Ca^{2+} . Whole-cell currents were measured at -60 mV membrane potential under the voltage clamp conditions, sampled at 10 kHz and filtered at 5 kHz (Axon 200B amplifier with pClamp software; Molecular Devices, LLC., San Jose, CA, USA). Heat stimulation was applied by increasing the bath temperature with a preheated solution. Temperature was monitored with a thermocouple (TA-29; Warner Instruments, Holliston, MA, USA) placed within 100 μm of the cell for current recording. For analysis of temperature thresholds, current densities were plotted on a log scale against the reciprocal of the absolute

temperature (T) in an Arrhenius plot and the temperature threshold was defined as the temperature at the intersection of the two extrapolated lines before and after channel activation. Q_{10} values were calculated using: $Q_{10} = I_{T+10}/I_T$ (I_{T+10} and I_T refer the current amplitude at $T+10^\circ\text{C}$ and $T^\circ\text{C}$) (Boukalova et al., 2010). The data in which the current was recovered to the basal level after removal of stimulation or which was completely inhibited by the TRPM2 inhibitor flufenamic acid (FFA, 500 μM) (Sigma, St. Louis, MO, USA) were used for analysis. Leak current <500 pA was set as the criterion for the data acceptance. Current peaks during stimulation subtracted from the current level recovered after stimulation or FFA inhibition were considered to be the current amplitude. All results were obtained from independent cells that were not exposed to repeated heat stimulations.

Statistical analysis

N represents the number of independent cells or cell lysate preparations from which results were obtained. The mean (SD) or median with corresponding range represented as lower-upper quartiles are shown as indicated. Figures show the mean (SD) or box-and-whisker plots with the mean (open circle), median (horizontal line), minimum and maximum values within the $1.5\times$ interquartile range (whiskers). Closed circles indicate individual data. Outliers were not excluded from the analyses. For normally distributed data (Kolmogorov–Smirnov), statistical analysis was performed using one-way or two-way ANOVA followed by a *post hoc* Dunnett's or Bonferroni-type multiple comparison as appropriate. Non-normally distributed data were analysed using Kruskal–Wallis one-way ANOVA followed by a *post hoc* Dunn's test. Statistical analyses were executed using Origin, version 9.9 (OriginLab, Northampton, MA, USA). $P < 0.05$ was considered statistically significant. Additional details regarding the statistical analyses are provided in the Statistical Summary Document.

Results

PMA treatment increased TRPM2 phosphorylation

Protein functions are modulated by many pathways under a variety of physiological and pathophysiological conditions. We previously reported that H_2O_2 , a reactive oxygen species involved in redox signalling, decreases temperature thresholds for transient receptor potential melastatin type 2 (TRPM2) channel activation. In the present study, we examined how phosphorylation of TRPM2 affected its temperature threshold. We first used phos-tag analysis to evaluate whether TRPM2 is phosphorylated by PKC or PKA. HEK293T cells expressing HA-tagged TRPM2 were treated with the

diacyl glycerol-mimetic PKC activator PMA (100 nM) or the PKA activator FK (10 μ M) for 20 min. At 0, 1, 2, 4 and 6 h after washout of PMA/FK, cell proteins were extracted for biochemical analyses. In phos-tag SDS-PAGE, the mobility of phosphorylated proteins is decreased, and bands corresponding to phosphorylated proteins can be observed in the upper positions of the gel relative to unphosphorylated proteins. The density of the upper bands (black arrowheads) observed in phos-tag SDS-PAGE continually increased from 1, 2, 4 and 6 h after PMA pretreatment (Fig. 1A). This PMA-induced increase in upper band density at 6 h after washout was completely abolished by treatment with λ PP, an enzyme that removes phosphorylation from Ser, Thr and Tyr residues (Fig. 1B). These data indicated that the bands could be specifically attributed to the phosphorylated TRPM2 protein, the levels of which were increased by the Ser/Thr kinase activity of PKC. Meanwhile, TRPM2 phosphorylation was not increased by FK treatment (Fig. 1A), suggesting that TRPM2 is targeted by PKC but not PKA. To normalise the amount of phosphorylated TRPM2 proteins, the density of the phosphorylated bands (black arrowheads) was divided by the total density of phosphorylated and unphosphorylated bands (grey arrowhead). TRPM2 phosphorylation was significantly increased beginning 1 h after PMA pretreatment and continued to increase after PMA pretreatment (Fig. 1C). The ratio of phosphorylated TRPM2 to total TRPM2 at 6 h after PMA pretreatment was 0.37 (0.08). In standard SDS-PAGE (Fig. 1A and B), the upper bands probably correspond to glycosylated proteins since the intensity was decreased in cell lysates treated with PNGase F (Fig. 1D) (Wehrhahn et al., 2010). The λ PP-treatment did not affect levels of this glycosylated protein (Fig. 1B), further suggesting that the phosphorylated form observed in phos-tag SDS-PAGE specifically reflects TRPM2 phosphorylation.

PMA treatment elevated the temperature threshold for TRPM2 activation

Temperature-dependent activation is a characteristic feature of TRPM2. We previously reported that redox signalling lowered the temperature threshold for TRPM2 activation to enable activation at body temperature (Kashio et al., 2012). To explore whether PMA-induced phosphorylation affects temperature-evoked activation of TRPM2, TRPM2-mediated currents were analysed in whole cells stimulated by heat in the presence of low concentrations of adenosine diphosphate ribose (ADPR, 3 and 10 μ M). At these low concentrations, ADPR does not promote TRPM2 activation at room temperature in the presence of 100 nM of intracellular free- Ca^{2+} (Starkus et al., 2007). Cells were used for patch clamp recordings within 2–3 h of PMA pretreatment

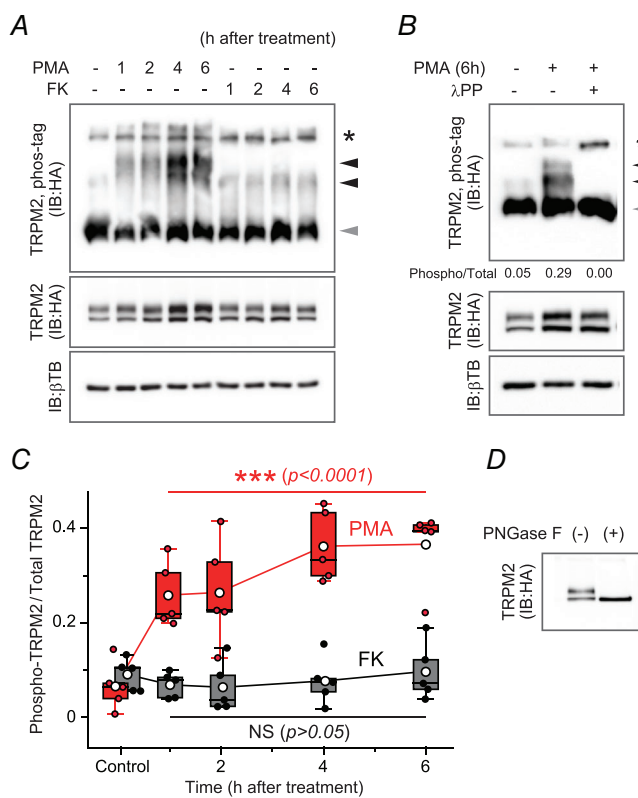


Figure 1. PMA-induced phosphorylation of TRPM2

A, phos-tag analysis of TRPM2 protein revealed PMA-induced phosphorylation of mouse TRPM2. HEK293T cells expressing HA-tagged mouse TRPM2 were treated with phorbol myristate acetate (PMA, 100 nM) or forskolin (FK, 10 μ M) for 20 min, and cultured in normal culture medium after washout of PMA or FK. Cell lysates were prepared 0, 1, 2, 4 and 6 h after PMA or FK pretreatment and the denatured protein samples were subjected to phos-tag SDS-PAGE. Phosphorylated (black arrowheads) and unphosphorylated (grey arrowhead) TRPM2 were separately observed in immunoblots of phos-tag SDS-PAGE. Signals in the upper regions indicated by asterisks could be attributed to multimers. Immunoblot signals of HA and β -tubulin in normal SDS-PAGE represent loading controls. B, PMA-induced phosphorylation of TRPM2 (6 h after PMA pretreatment) was abolished by lambda protein phosphatase (λ PP)-treatment. The values below the phos-tag SDS-PAGE indicate the ratios of phosphorylated TRPM2/total TRPM2 in the corresponding lane. C, time-course of changes in TRPM2 phosphorylation caused by PMA (red) or FK (black)-pretreatment. The ratio of phosphorylated TRPM2/total TRPM2 was calculated using immunoblot signals detected in phos-tag SDS-PAGE. Box-and-whisker plots with mean (open circles) and individual data (closed circles) ($N = 5$). Results were analysed by two-way ANOVA followed by a *post hoc* Dunnett's multiple comparison ($^{NS}P \geq 0.05$, $^{***}P < 0.001$ vs. 0 h of corresponding group). Relative to control for PMA, the P values were $P = 1.40 \times 10^{-5}$, $P = 9.59 \times 10^{-6}$, $P = 2.93 \times 10^{-8}$ and $P = 2.30 \times 10^{-8}$ for 1, 2, 4 and 6 h after PMA treatment, respectively. Relative to control for FK, P values were $P = 0.544$, $P = 0.370$, $P = 0.836$ and $P > 0.999$ for 1, 2, 4 and 6 h after FK treatment, respectively. Additional details about the statistical analyses are provided in the Statistical Summary Document. D, N-glycosylation of TRPM2. The upper band of TRPM2 observed in normal SDS-PAGE was eliminated by treatment with peptide-N-glycosidase F (PNGase F). [Colour figure can be viewed at wileyonlinelibrary.com]

because longer culture periods after PMA pretreatment increased TRPM2 expression following phosphorylation of large T antigens expressed in HEK293T cells. Heat stimulation caused robust activation of TRPM2 currents with desensitisation occurring in the absence [PMA(-)] and presence [PMA(+)] of PMA pretreatment (Fig. 2A and B). Residual currents observed after the temperature decrease were completely inhibited by FFA (500 μM) treatment, suggesting that these currents were a result of TRPM2 activation induced by continuous Ca²⁺ influx

through TRPM2 channels (Fig. 2A and B). Representative Arrhenius plots of heat-evoked TRPM2 currents showed that both PMA(-) and PMA(+) traces had apparent flexion points of temperature-dependence that indicate temperature thresholds (Fig. 2C). Surprisingly, PMA pretreatment caused a substantial increase in the temperature threshold for TRPM2 activation from 36.9°C to 43.4°C (Fig. 2A–C). Temperature coefficients (Q₁₀) to evaluate temperature-dependence of reactions are calculated as the fold-increase of current amplitudes when temperature is

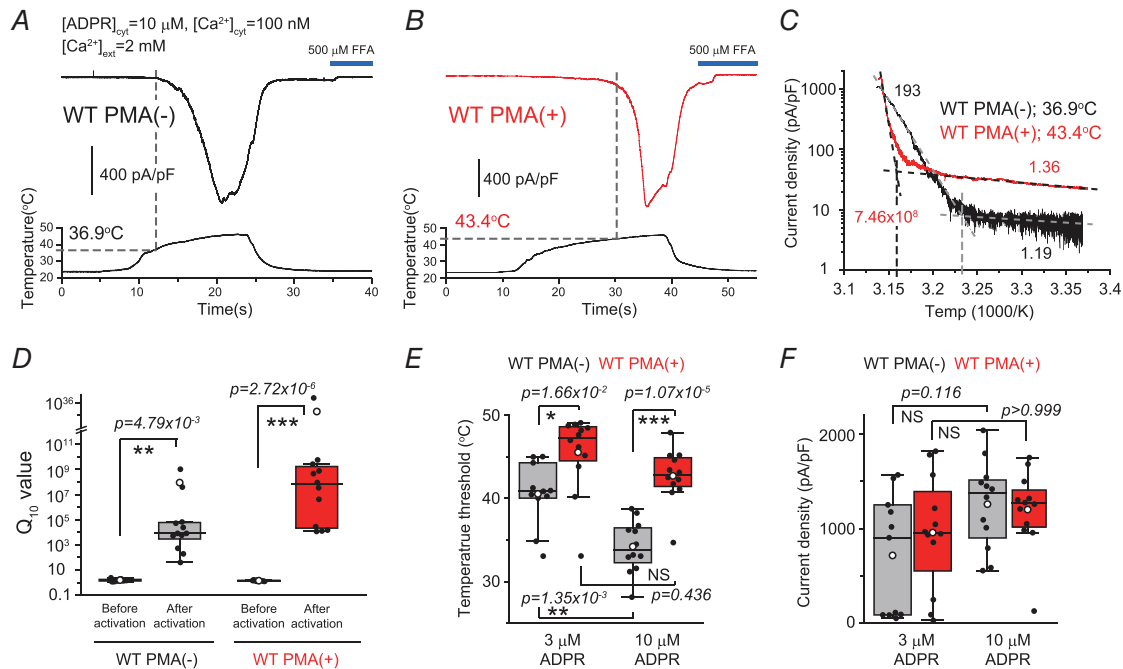


Figure 2. PMA-induced elevation of temperature threshold for TRPM2 activation
 A and B, heat-evoked TRPM2 current recorded using a pipette solution containing adenosine diphosphate ribose (ADPR, 10 μM) and Ca²⁺ (100 nM), and extracellular bath solution containing 2 mM Ca²⁺. PMA(-) and PMA(+) traces indicate TRPM2 current without (black, A) or with PMA pretreatment (red, B), respectively. PMA treatment (100 nM 20 min) was applied 2–3 h before the current recordings. Upper traces indicate current density (pA/pF) of TRPM2 recorded at a holding potential of V_m = -60 mV. Lower traces indicate temperature transition. Flufenamic acid (FFA, 500 μM), a TRPM2 inhibitor, was added to inhibit sustained currents. Dashed lines indicate inflection points of the Arrhenius plots shown in (C). C, Arrhenius plots of heat-evoked currents of TRPM2 without (black, A) or with (red, B) PMA pretreatment. The relationship between the inverse of the absolute temperature (1000/K) and logarithmic current density (pA/pF) was plotted to analyse temperature thresholds. Dashed lines show the regression of each trace, and the intersections indicate temperature thresholds. Calculated temperature thresholds and Q₁₀ values before and after reaching the thresholds are shown for each trace. D, Q₁₀ values before and after reaching the temperature threshold for TRPM2 activation. Q₁₀ values were calculated using heat-evoked TRPM2 currents in the presence of cytosolic Ca²⁺ (100 nM) and ADPR (10 μM), and extracellular Ca²⁺ (2 mM). PMA(-) (black) and PMA(+) (red) indicate the condition without or with PMA pretreatment, respectively. Box-and-whisker plots with mean (open circles) and individual data (closed circles) (N = 10–12) are shown. Results were analysed by Kruskal-Wallis ANOVA followed by a *post hoc* Dunn's test (P between indicated pairs). E, PMA-induced elevation of TRPM2 thresholds. Temperature thresholds were calculated using TRPM2 activation without (black, A) or with (red, B) PMA pretreatment. PMA pretreatment significantly elevated temperature thresholds of heat-evoked TRPM2 currents in the presence of 3 and 10 μM ADPR. Box-and-whisker plots with mean (open circles) and individual data (closed circles) (N = 11–12). Results were analysed by two-way ANOVA followed by a *post hoc* Bonferroni-type multiple comparison (P between indicated pairs). F, PMA pretreatment did not affect amplitudes of heat-evoked TRPM2 currents. No significant change was observed among the tested conditions. Box-and-whisker plots with mean (open circles) and individual data (closed circles) (N = 11–12) are shown. Results were analysed by two-way ANOVA followed by a *post hoc* Bonferroni-type multiple comparison (P between indicated pairs). Additional details about the statistical analyses are provided in the Statistical Summary Document. [Colour figure can be viewed at wileyonlinelibrary.com]

increased by 10°C ($Q_{10} = I_{T+10}/I_T$). For ion channels not activated by temperature, Q_{10} values are 2 to 3 (Bertil, 2001). At a temperature below the threshold for TRPM2 activation, Q_{10} values were low for both PMA(–) and PMA(+) (1.50, range 1.37–1.75 and 1.44, range 1.38–1.54, respectively) (Fig. 2D), which corresponds to Q_{10} values that reflect temperature-dependent ion diffusion (1.2–1.5) (Bertil, 2001). However, after reaching the temperature threshold for TRPM2, the Q_{10} values markedly increased regardless of PMA treatment (8.24×10^3 , range 4.07×10^3 to 5.64×10^4 and 6.22×10^7 , range 2.48×10^4 to 1.21×10^9 , respectively) (Fig. 2D), indicating a clear temperature-evoked activation of TRPM2.

The temperature threshold for PMA(–) was lower in cells treated with 10 μM ADPR compared to those treated with 3 μM ADPR [34.2 (3.1)°C vs. 40.6 (3.8)°C] (Fig. 2E). A significant elevation in the temperature thresholds for TRPM2 activation was achieved with PMA pretreatment in the presence of either 3 or 10 μM ADPR, and the elevation for 10 μM ADPR was larger ($P = 1.07 \times 10^{-5}$) than that for 3 μM ADPR ($P = 1.66 \times 10^{-2}$) (Fig. 2E). By contrast, heat-evoked current amplitudes were not affected by PMA pretreatment (Fig. 2F), although the amplitudes for these currents did exhibit broad variability. These data suggested that PMA-induced phosphorylation of TRPM2 modifies temperature thresholds for TRPM2 activation without affecting current amplitudes.

PMA treatment counteracted cytosolic Ca^{2+} -dependent reduction in temperature threshold for TRPM2 activation

TRPM2 activation increases intracellular Ca^{2+} that is mediated by Ca^{2+} influx through the activated channel pore. Intracellular Ca^{2+} ions have indispensable roles for TRPM2 activation, and TRPM2 activation does not occur in the complete absence of Ca^{2+} even in the presence of high concentrations of ADPR (McHugh et al., 2003). Recent studies using cryo-electron microscopy (cryo-EM) revealed a Ca^{2+} binding site in the cytosolic cleft of TRPM2 TM domains (Huang et al., 2018, 2019; Wang et al., 2018). This Ca^{2+} binding site is thought to play a critical role in TRPM2 activation (Csanady & Torocsik, 2009). Therefore, we next investigated how cytosolic Ca^{2+} affects the temperature thresholds for TRPM2 activation.

To strictly fix cytosolic Ca^{2+} concentrations, heat-evoked TRPM2 currents were measured using an intracellular solution containing target concentrations of free Ca^{2+} (buffered with 5 mM EGTA) under extracellular Ca^{2+} -free (5 mM EGTA) conditions. In the presence of 10 μM ADPR, a temperature increase evoked TRPM2 current activation (Fig. 3A). PMA-induced elevation of the temperature thresholds for TRPM2 activation was also observed when the cytosolic Ca^{2+} concentration was fixed at 100 μM (Fig. 3A and B), which is consistent

with the result obtained in the presence of extracellular Ca^{2+} that allows Ca^{2+} influx and increases in local cytosolic Ca^{2+} near the activated TRPM2 channel pore. Q_{10} values for heat-evoked TRPM2 currents recorded with 100 μM fixed cytosolic Ca^{2+} concentration were lower than those observed in the presence of 2 mM extracellular Ca^{2+} for both PMA(–) and PMA(+) (1.10×10^2 , range 60.1 to 3.03×10^2 and 2.32×10^2 , range 1.18×10^2 to 5.90×10^6 , respectively) (Fig. 3C). These results suggested that influx of extracellular Ca^{2+} strongly enhances TRPM2 activation to increase Q_{10} values. Despite the changes in Q_{10} values, a similar effect of PMA on temperature thresholds was observed, further supporting the preferential effect of PMA on TRPM2 temperature thresholds. These data obtained with fixed cytosolic Ca^{2+} concentrations explicitly exclude the possibility that PMA-induced elevation in the temperature thresholds for TRPM2 activation could be attributed to changes in Ca^{2+} permeability of the TRPM2 pore or in a consequent increase in local Ca^{2+} concentrations near the membrane. Moreover, temperature thresholds for TRPM2 activation were significantly decreased along with elevation of intracellular Ca^{2+} concentrations from 0.1 to 100 μM without PMA pretreatment (Fig. 3D and F). Surprisingly, the Ca^{2+} -dependent decrease in temperature thresholds was completely abolished at all examined cytosolic Ca^{2+} concentrations (0.1, 1, 10 and 100 μM) after PMA pretreatment (2 h after washout) (Fig. 3E and F). Arrhenius plots of heat-evoked currents in the presence of 0.1, 1, 10 or 100 μM cytosolic Ca^{2+} showed clear differences between cells that were and were not pretreated with PMA (Fig. 3D and E). As a result, in the presence of 10 and 100 μM cytosolic Ca^{2+} , temperature thresholds for TRPM2 activation were significantly higher [43.7 (2.9)°C and 42.8 (4.4)°C, respectively] in PMA-treated cells than in untreated cells [38.9 (3.9)°C and 34.6 (3.5)°C, respectively] (Fig. 3A, B and F). Elevation in the cytosolic Ca^{2+} concentration also increased current amplitudes, although this increase was not affected by PMA pretreatment (Fig. 3G). These data taken together suggested that Ca^{2+} binding to the intracellular domain of TRPM2 contributes to increases in current amplitudes and decreases in temperature thresholds for heat-evoked TRPM2 activation. PMA-induced phosphorylation of TRPM2 could counteract cytosolic Ca^{2+} -dependent changes in temperature thresholds without affecting amplitudes of heat-evoked TRPM2 currents.

Candidate amino acid residues involved in TRPM2 phosphorylation

The above results indicate that TRPM2 phosphorylation substantially affects its activity. To identify the amino acid residue(s) involved in PMA-induced TRPM2 phosphorylation, we introduced alanine substitutions

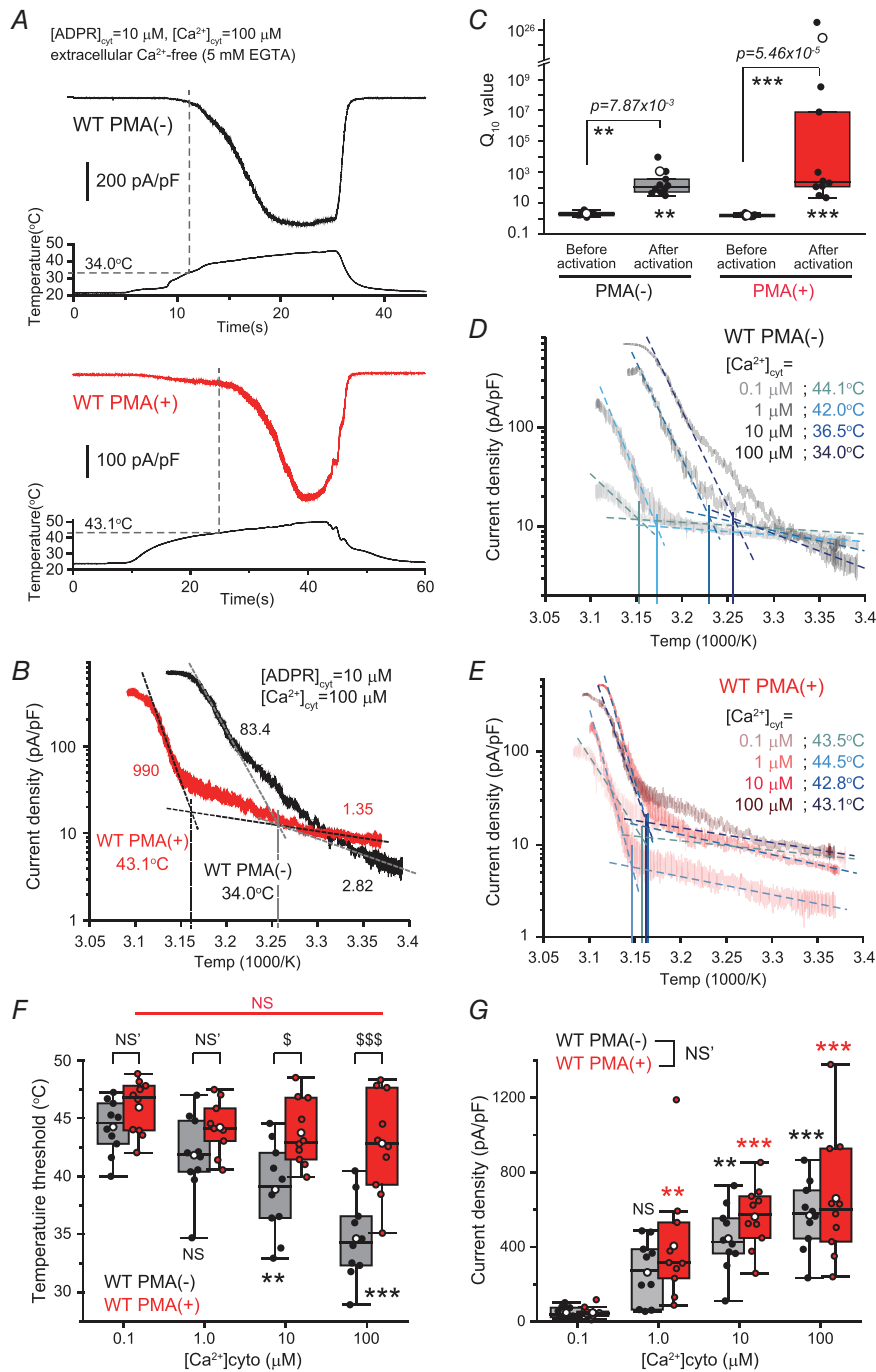


Figure 3. PMA treatment abolished cytosolic Ca²⁺-induced reduction of temperature threshold for TRPM2 activation

A, heat-evoked TRPM2 currents recorded using pipette solution containing ADPR (10 μM) and Ca²⁺ (100 μM) under extracellular Ca²⁺-free (5 mM EGTA) conditions. PMA(–) and PMA(+) traces indicate TRPM2 current without (black, A) or with PMA pretreatment (red, B), respectively. PMA treatment (100 nM, 20 min) was applied 2–3 h before the current recordings. Upper traces indicate current densities (pA/pF) of TRPM2 recorded at the holding potential ($V_m = -60$ mV). Lower traces indicate temperature transition. B, arrhenius plots of heat-evoked TRPM2 currents shown in (A). Arrhenius plots, calculated temperature thresholds and Q_{10} values before and after reaching threshold for PMA(–) (black) and PMA(+) (red) are shown. C, Q_{10} values before and after reaching the temperature threshold for TRPM2 activation. Q_{10} values were calculated using heat-evoked TRPM2 currents recorded in the presence of cytosolic Ca²⁺ (100 μM) and ADPR (10 μM) under extracellular Ca²⁺-free conditions. PMA(–) (black) and PMA(+) (red) indicate that the cells did not or did, respectively, have PMA pretreatment. Box-and-whisker plots

with mean (open circles) and individual data (closed circles) ($N = 10$ – 12) are shown. Results were analysed by a Kruskal–Wallis ANOVA followed by a *post hoc* Dunn's test (P between indicated pairs). *D*, reduction in temperature thresholds for TRPM2 activation depending on cytosolic Ca^{2+} concentration. Arrhenius plots show the relationship of temperature–current densities obtained for heat-evoked currents in the presence of cytosolic Ca^{2+} from 0.1 to 100 μM (from light to dark grey). All traces were recorded in the presence of cytosolic ADPR (10 μM) under extracellular Ca^{2+} -free conditions. The regression lines and calculated threshold values for each trace are shown (from 0.1 to 100 μM Ca^{2+} ; from light to dark blue). *E*, cytosolic Ca^{2+} -dependent reduction of TRPM2 thresholds abrogated by PMA pretreatment. Arrhenius plots of heat-evoked TRPM2 currents recorded 2–3 h after PMA pretreatment under conditions corresponding to those in (C). *F*, effect of cytosolic Ca^{2+} and PMA pretreatment on temperature thresholds of heat-evoked TRPM2 activation in the presence of cytosolic ADPR (10 μM) and Ca^{2+} at the indicated concentrations under extracellular Ca^{2+} -free (5 mM EGTA) conditions. PMA(–) (black) and PMA(+) (red) indicate the presence and absence of PMA pretreatment, respectively. Box-and-whisker plots with mean (open circles) and individual data (closed circles) ($N = 10$). $^{\text{NS}}P \geq 0.05$, $^{**}P < 0.01$, $^{***}P < 0.001$ vs. 0.1 μM Ca^{2+} of the corresponding group. $^{\text{NS}}P \geq 0.05$, $^{\text{S}}P < 0.05$, $^{\text{SSS}}P < 0.001$ between indicated pairs. Results were analysed by two-way ANOVA followed by a *post hoc* Bonferroni-type multiple comparison. The P values for PMA(–) compared to 0.1 μM Ca^{2+} were $P > 0.999$, $P = 9.87 \times 10^{-3}$ and $P = 1.15 \times 10^{-7}$ for 1.0, 10 and 100 μM Ca^{2+} . The P values for PMA(+) compared to 0.1 μM Ca^{2+} were $P > 0.999$, $P > 0.999$ and $P = 0.953$ for 1.0, 10 and 100 μM Ca^{2+} . The P values in comparisons between PMA(–) and PMA(+) were $P > 0.999$, $P > 0.999$, $P = 3.27 \times 10^{-2}$ and $P = 7.33 \times 10^{-6}$ for 0.1, 1.0, 10 and 100 μM Ca^{2+} , respectively. Additional details about the statistical analyses are provided in the Statistical Summary Document. *G*, effect of cytosolic Ca^{2+} and PMA pretreatment on current amplitudes of heat-evoked TRPM2 activation under conditions corresponding to those in (F). Box-and-whisker plots with mean (open circles) and individual data (closed circles) ($N = 10$). $^{\text{NS}}P \geq 0.05$, $^{**}P < 0.01$, $^{***}P < 0.001$ vs. 0.1 μM Ca^{2+} of the corresponding group. Results were analysed by two-way ANOVA followed by a *post hoc* Bonferroni-type multiple comparison. The P values for PMA(–) compared to 0.1 μM Ca^{2+} were $P = 0.610$, $P = 1.45 \times 10^{-3}$ and $P = 8.34 \times 10^{-6}$ for 1.0, 10 and 100 μM Ca^{2+} , respectively. The P values for PMA(+) compared to 0.1 μM Ca^{2+} were $P = 6.46 \times 10^{-3}$, $P = 1.12 \times 10^{-5}$ and $P = 1.40 \times 10^{-7}$, for 1.0, 10 and 100 μM Ca^{2+} , respectively. Additional details about the statistical analyses are provided in the Statistical Summary Document. [Colour figure can be viewed at wileyonlinelibrary.com]

at Ser/Thr residues that could be targeted by PKC (NetPhos-3.1). In total, 36 intracellular candidate Ser/Thr residues are present in the TRPM2 N- and C-terminal regions. For the mutations T290A, T416A, T689A and T738A, the PMA-induced increase in phosphorylated TRPM2 protein was significantly decreased (black arrowheads in Fig. 4A and B), indicating candidate residues for PMA-induced TRPM2 phosphorylation. The mutant T689A had low expression [1.9 (2.2)% of WT TRPM2] and was not analysed further.

Potential involvement of Thr738 phosphorylation in counteracting the effect of cytosolic Ca^{2+} on temperature thresholds for TRPM2 activation

To confirm functional expression of mutant channels, ADPR (300 μM)-evoked currents for TRPM2 carrying T290A, T416A or T738A mutations were evaluated in the presence of cytosolic Ca^{2+} (100 nM) and extracellular Ca^{2+} (2 mM) at room temperature. T738A exhibited robust ADPR-evoked currents that were comparable to WT channels, and these currents were reversibly inhibited by FFA (Fig. 5A and B). On the other hand, T290A and T416A showed negligible current activation (Fig. 5B). A phospho-mimic mutation of T738 to aspartic acid (T738D) also showed ADPR-evoked currents (Fig. 5A and B). These data confirmed that channel function of T738A and T738D was preserved. Next, further studies were conducted to examine the involvement of T738 in

PMA-induced elevation of temperature thresholds for TRPM2 activation. A cytosolic Ca^{2+} -dependent reduction in the temperature thresholds and an increase in current amplitudes were observed for the T738A mutant that were similar to those seen for WT channels (Fig. 5D and E). However, PMA pretreatment did not increase the temperature threshold of T738A TRPM2 activation at all cytosolic Ca^{2+} concentrations between 0.1 and 100 μM , and the PMA effect on the temperature threshold for the T738A mutant was abolished (Fig. 5C and D). The phospho-mimic T738D mutant showed small current activation for cytosolic Ca^{2+} concentrations ranging from 1.0 to 100 μM , whereas the high-temperature threshold similar to that of PMA-treated WT channel was maintained (Fig. 5F and G). Because the lower current activation could be attributed to the low Ca^{2+} -sensitivity of the T738D mutant, a higher concentration of cytosolic Ca^{2+} (1 mM) was applied to this mutant channel. Consistent with the hypothesis, a temperature increase drove large current activation of T738D channel in the presence of 1 mM cytosolic Ca^{2+} , although the temperature threshold for T738D activation remained high (Fig. 5C, F and G). These data suggested that T738 is involved in phosphorylation-mediated elevation of temperature thresholds for TRPM2 activation. Moreover, the data showing that temperature thresholds and current amplitudes were differently modulated by cytosolic Ca^{2+} probably excludes the possibility that changes in the temperature thresholds were caused by differences in current amplitudes.

Discussion

An important feature of TRP channels is temperature sensitivity. A wide range of temperatures from noxious cold to noxious heat is detected by many thermo-TRPs, which are each sensitive to particular temperatures. The temperature thresholds for activation of many thermo-TRPs can be regulated by various factors. Temperature thresholds for TRPV1, a noxious heat sensor, are lowered by PKA/PKC-mediated phosphorylation induced by inflammation. This reduction in the temperature threshold for TRPV1 activation allows activation at body temperature and is associated with

inflammatory hyperalgesia (Moriyama et al., 2005; Numazaki et al., 2002; Rathee et al., 2002; Vellani et al., 2001). Although many candidate amino acid residues were reported to be involved in this phosphorylation-induced elevation in heat sensitivity (Moriyama et al., 2005; Numazaki et al., 2002; Rathee et al., 2002), the detailed mechanisms regulating the temperature thresholds of TRPV1 channels remain largely unknown, as is how temperature-dependent activation of thermo-TRPs with a characteristic temperature threshold is achieved.

In addition to temperature, TRPM2 activity is regulated by multiple factors, including cytosolic Ca²⁺ and the endogenous agonist ADPR (Kashio & Tominaga, 2017).

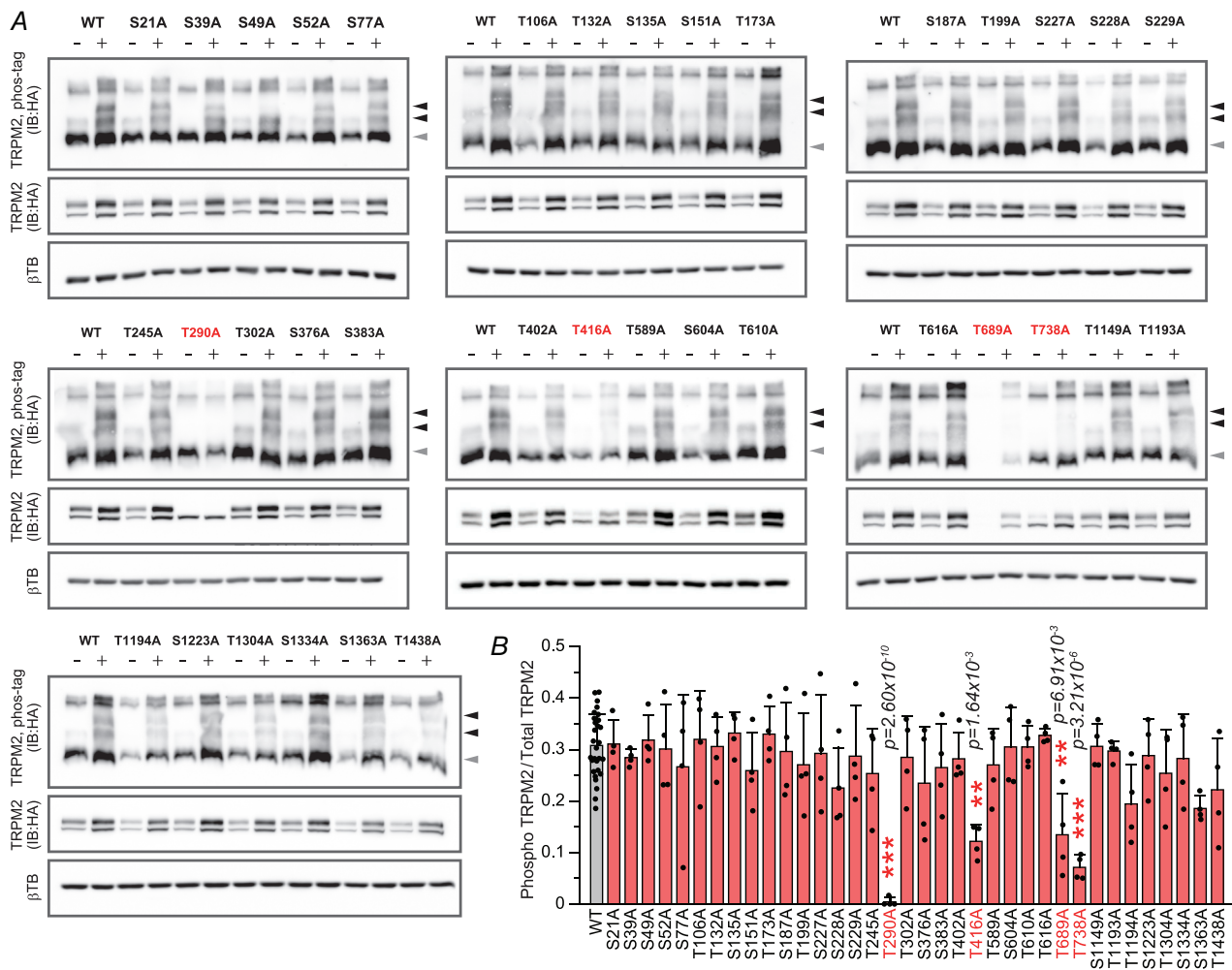


Figure 4. Alanine scanning mutagenesis of Ser/Thr residues at potential PMA-induced phosphorylation sites in TRPM2
 A, phos-tag analysis detecting phosphorylated TRPM2 without (–) or with (+) PMA pretreatment (6 h after washout). Phosphorylated and unphosphorylated TRPM2 are indicated by black and grey arrowheads, respectively. Mutants showing significant reduction of phosphorylated protein are highlighted with red text. B, effect of alanine substitutions on phosphorylated/total TRPM2. TRPM2 phosphorylation was significantly reduced in TRPM2 mutants T290A, T416A and T738A (mean ± SD). Individual data points are indicated by black circles (N = 29 for WT, N = 4 for mutants). Results were analysed by one-way ANOVA followed by a *post hoc* Bonferroni-type multiple comparison (*P* vs. WT). No statistical significance was observed (*P* > 0.999 vs. WT) unless noted. Additional details about the statistical analyses are provided in the Statistical Summary Document. [Colour figure can be viewed at wileyonlinelibrary.com]

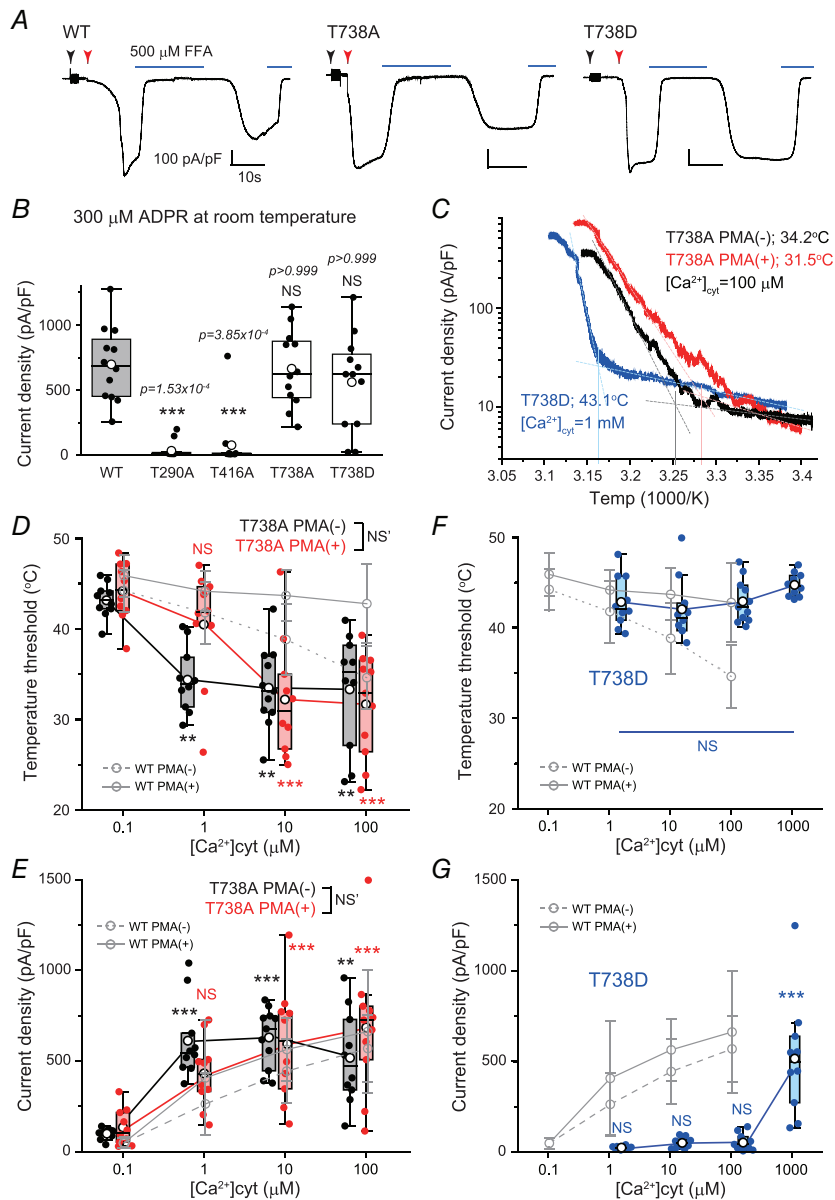


Figure 5. T738 phosphorylation in TRPM2 potentially mediates PMA-induced reduction of TRPM2 threshold

A, representative traces of ADPR (300 μM)-evoked current activation for WT TRPM2 and TRPM2 with T738A or T738D mutations. Whole-cell configuration using pipette solution containing ADPR was established at time points indicated by black arrowheads, and the cells were voltage clamped ($V_m = -60$ mV) at time points indicated by red arrowheads. FFA (500 μM , blue bars) was applied to inhibit TRPM2 currents. Scale bars indicate 10 s (horizontal) and 100 pA/pF (vertical). B, ADPR (300 μM)-evoked current amplitudes of WT, T290A, T416A, T738A and T738D TRPM2. T738A and T738D TRPM2 showed substantial current activation compared to WT channels, whereas ADPR-evoked currents for TRPM2 with T290A and T416A mutations were significantly abrogated. Box-and-whisker plots show the mean (open circles) and individual data points (closed circles) ($N = 12\text{--}13$). Results were analysed by Kruskal-Wallis ANOVA followed by a *post hoc* Dunn's test (P vs. WT). C, Arrhenius plots of heat-evoked currents of T738A mutant without (–) (black) and with (+) PMA pretreatment (red) in the presence of cytosolic Ca^{2+} (100 μM) and of T738D without PMA pretreatment (blue) in the presence of cytosolic Ca^{2+} (1 mM). PMA treatment (100 nM, 20 min) was applied 2–3 h before the current recordings. All current traces were recorded in the presence of cytosolic ADPR (10 μM) and under extracellular Ca^{2+} -free conditions (5 mM EGTA). Calculated threshold values for each trace are shown. D, effect of cytosolic Ca^{2+} and PMA pretreatment on temperature thresholds of heat-evoked TRPM2 T738A activation in the presence of cytosolic ADPR (10 μM) and Ca^{2+} at the indicated concentration under extracellular Ca^{2+} -free (5 mM EGTA) conditions. PMA(–) and PMA(+) indicate the condition without (black) or with PMA pretreatment (red), respectively.

Box-and-whisker plots indicate the mean (open circles) and individual data points (closed circles) ($N = 10-11$). The data obtained for WT channels are shown as grey traces for purposes of comparison (mean \pm SD). $^{NS}P \geq 0.05$, $^{**}P < 0.01$, $^{***}P < 0.001$ vs. $0.1 \mu\text{M Ca}^{2+}$ of the corresponding group. $^{NS}P \geq 0.05$ between PMA(-) and PMA(+). Results were analysed by two-way ANOVA followed by a *post hoc* Bonferroni-type multiple comparison. For PMA(-), P values determined for comparisons with $0.1 \mu\text{M Ca}^{2+}$ were 6.25×10^{-3} , 1.07×10^{-3} and $P = 1.18 \times 10^{-3}$ for 1.0, 10 and $100 \mu\text{M Ca}^{2+}$, respectively. For PMA(+), the values for the same comparison were $P > 0.999$, $P = 3.16 \times 10^{-5}$ and $P = 7.48 \times 10^{-6}$ for 1.0, 10 and $100 \mu\text{M Ca}^{2+}$, respectively. *E*, effect of cytosolic Ca^{2+} and PMA pretreatment on current amplitudes of heat-evoked TRPM2 T738A activation under conditions corresponding to those in (D). Box-and-whisker plots show the mean (open circles) and individual data points (closed circles) ($N = 10-11$). The data obtained for WT channels are shown as grey traces for purposes of comparison (mean \pm SD). $^{NS}P \geq 0.05$, $^{**}P < 0.01$, $^{***}P < 0.001$ vs. $0.1 \mu\text{M Ca}^{2+}$ of corresponding group. $^{NS}P \geq 0.05$ between PMA(-) and PMA(+). Results were analysed by two-way ANOVA followed by a *post hoc* Bonferroni-type multiple comparison. For PMA(-), P values determined for comparisons with $0.1 \mu\text{M Ca}^{2+}$ were $P = 1.08 \times 10^{-4}$, $P = 3.42 \times 10^{-5}$ and $P = 3.23 \times 10^{-3}$ for 1.0, 10 and $100 \mu\text{M Ca}^{2+}$, respectively. For PMA(+), the values for the same comparison were $P = 0.138$, $P = 7.57 \times 10^{-4}$ and $P = 1.55 \times 10^{-5}$ for 1.0, 10 and $100 \mu\text{M Ca}^{2+}$, respectively. *F*, effect of cytosolic Ca^{2+} and PMA pretreatment on temperature thresholds of heat-evoked T738D activation (blue) in the presence of cytosolic ADPR ($10 \mu\text{M}$) and Ca^{2+} at the indicated concentration under extracellular Ca^{2+} -free (5 mM EGTA) conditions. Box-and-whisker plots show the mean (open circles) and individual data points (closed circles) ($N = 10-11$). The data obtained for WT channels are shown as grey traces for purposes of comparison (mean \pm SD). No statistical significance was observed among 1.0, 10, $100 \mu\text{M}$ and 1 mM Ca^{2+} in T738D ($P = 0.143$, one-way ANOVA). *G*, the effect of cytosolic Ca^{2+} and PMA pretreatment on current amplitudes of heat-evoked T738D activation (blue) under conditions corresponding to those in (F). Box-and-whisker plots show the mean (open circles) and individual data points (closed circles) ($N = 10-11$). The data obtained for WT channels are shown as grey traces for purposes of comparison (mean \pm SD). $^{NS}P \geq 0.05$, $^{***}P < 0.001$ vs. $1 \mu\text{M Ca}^{2+}$. Results were analysed by one-way ANOVA followed by a *post hoc* Bonferroni-type multiple comparison. Compared with $1 \mu\text{M Ca}^{2+}$, P values were $P > 0.999$, $P > 0.999$ and $P = 3.20 \times 10^{-7}$ for $10 \mu\text{M}$, $100 \mu\text{M}$ and 1 mM Ca^{2+} , respectively. Additional details about the statistical analyses are provided in the Statistical Summary Document. [Colour figure can be viewed at wileyonlinelibrary.com]

Cytosolic Ca^{2+} has an indispensable role in TRPM2 activation and, even at high concentrations, ADPR itself cannot activate TRPM2 in the complete absence of extracellular and cytosolic Ca^{2+} (McHugh et al., 2003). TRPM2 has been reported to have an isoleucine–glutamine-like calmodulin binding motif in the N-terminus (Tong et al., 2006). Coexpression of mutant calmodulin lacking a Ca^{2+} -binding motif decreased TRPM2 activation, suggesting functional augmentation of TRPM2 by Ca^{2+} -calmodulin binding. High-resolution cryo-EM studies to determine the tertiary structure of TRPM2 revealed a Ca^{2+} binding site in the TM domain of TRPM2 (Huang et al., 2018, 2019; Wang et al., 2018). Furthermore, in structures of humans and zebrafish TRPM2, a Ca^{2+} binding pocket formed by Glu/Gln/Asn/Asp residues in the TM segment, S2 and S3, and a Glu residue in the TRP domain is apparent (Fig. 6). These amino acid residues are conserved across invertebrates and vertebrates, including mouse TRPM2. Ca^{2+} binding to this site in the TM domain is considered to induce conformational changes in the S1–S4 and TRP helix that are followed by movement of pore-forming S5–S6 helices and channel opening (Fig. 6) (Huang et al., 2018, 2019; Wang et al., 2018). These structural studies also indicate how ADPR binds to TRPM2 of different species. ADPR is suggested to bind to two sites, the N-terminal TRPM homology region 1/2 (MHR1/2) and the C-terminal ADP-ribose pyrophosphatase homology (NUDT9H) domain. In human TRPM2, both sites may be involved in ADPR binding (Huang et al., 2019), whereas, in zebrafish and sea anemone TRPM2, only MHR1/2

appears to play a role (Huang et al., 2018, 2019). ADPR binding to these sites causes structural changes in the cytosolic domain that are transmitted to the TM domain through the movement of MHR3/4 and TRP helix. Because of the indispensable roles for Ca^{2+} in TRPM2 activity (Csanady & Torocsik, 2009; McHugh et al., 2003),

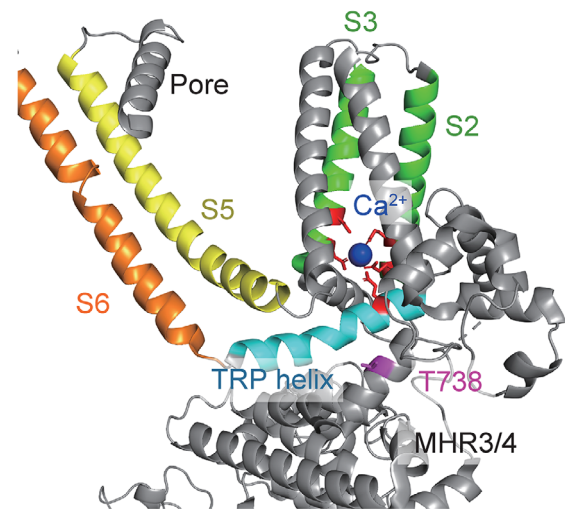


Figure 6. Predicted location of Thr738 in the tertiary structure of mouse TRPM2 (adapted human TRPM2, PDB ID; 6pus) Thr738 (T738, magenta); Ca^{2+} (blue); Ca^{2+} binding pocket (red) formed by the TRP helix (cyan), S2 and S3 (green); S5 (yellow) and S6 (orange) of a single subunit are highlighted. The structure was prepared using the PyMOL Molecular Graphics System, version 2.0 (Schrödinger, LLC, New York, NY, USA). [Colour figure can be viewed at wileyonlinelibrary.com]

ADPR and Ca^{2+} binding at these sites is considered to co-ordinately lead to conformational changes in the entire structure of TRPM2 and subsequently promote opening of the channel pore.

The results of the present study reveal a new regulatory mechanism for temperature thresholds for TRPM2 activation where cytosolic Ca^{2+} decreases the thresholds in a concentration-dependent manner, and this decrease can be counteracted by TRPM2 phosphorylation (Fig. 3). The high Ca^{2+} permeability of TRPM2 allows increases in cytosolic Ca^{2+} to further augment channel activity. In addition, the data showing that cytosolic Ca^{2+} decreases the temperature threshold for TRPM2 activation (Fig. 3D and F) suggest that TRPM2 activity at body temperature could be elevated by increases in local Ca^{2+} near the cytosolic Ca^{2+} binding site. Temperature thresholds for TRPM2 activation were in the physiological temperature range in the presence of extracellular Ca^{2+} (2 mM) with cytosolic Ca^{2+} (100 nM) and ADPR (10 μM) (Fig. 2E). The thresholds corresponded to those observed for the condition of fixed cytosolic Ca^{2+} concentrations at 10–100 μM (Fig. 3F). These data suggest that the local Ca^{2+} concentrations in the Ca^{2+} binding site could be between 10 and 100 μM , consistent with a previous report (Csanady & Torocsik, 2009).

We also identified candidate amino acids involved in PMA-induced changes in temperature thresholds for TRPM2 activation. The T290 residue is considered to be in the vicinity of the ADPR binding pocket in MHR1/2 and is conserved in both humans and zebrafish TRPM2 (Huang et al., 2018, 2019; Wang et al., 2018). ADPR-evoked current activation for the T290A mutant was largely diminished (Fig. 5B), as was reported for human TRPM2 (Luo et al., 2018), which suggests the importance of this threonine for ADPR-induced channel activation. The T416 residue is in the isoleucine–glutamine-like motif (Tong et al., 2006) and could have roles in functional regulation of TRPM2 by Ca^{2+} , although the channel function of T416A mutant was largely affected (Fig. 5B). Moreover, alanine substitution of T689 in MHR4 resulted in almost no protein expression at the basal level [1.9 (2.2)% of WT TRPM2]. As a result of the negligible current amplitudes or protein expression, the effects of alanine mutations at T290, T416 and T689 on PMA-induced regulation of temperature thresholds could not be evaluated.

Alanine substitution at T738 and the phosphomimic T738D maintained channel function comparable to that for the WT channel (Fig. 5A and B). The effect of PMA on temperature thresholds was completely abolished in T738A, whereas the phosphomimic T738D mutant phenocopied the PMA effect on WT temperature thresholds (Fig. 5C, D and F). The T738D mutant showed very small current amplitudes even at 100 μM intracellular Ca^{2+} ; however, robust current activation was

achieved in the presence of 1 mM Ca^{2+} (Fig. 5G). These results indicate that the T738D mutation could decrease the potency of cytosolic Ca^{2+} to its binding site in TRPM2. Furthermore, the T738 residue is a potential phosphorylation site that could modulate the effect of cytosolic Ca^{2+} on temperature thresholds for TRPM2. The T738 residue is located in the MHR4 domain of TRPM2. MHR4 faces the TRP helix, and T738 is close to the Glu residue in the TRP helix that is involved in Ca^{2+} binding to the cytosolic cleft of TM domain, as mentioned above (Fig. 6) (Huang et al., 2018, 2019; Wang et al., 2018). Phosphorylation of T738 could therefore introduce bulky negative charges at this site. Our observation that TRPM2 phosphorylation counteracts the effect of cytosolic Ca^{2+} on reducing temperature thresholds could be interpreted as a change in Ca^{2+} affinity for the binding pocket formed by S2–S3 of the TM and TRP helix. This possibility is supported by the result showing that not only the T738A mutation abolished the effect of PMA, but also the phosphomimic T738D mutation phenocopied the effect of PMA to elevate temperature thresholds regardless of cytosolic Ca^{2+} concentration (Fig. 5D and F).

In the present study, we carried out a systematic analysis under fixed cytosolic Ca^{2+} conditions to explore how cytosolic Ca^{2+} affected the temperature threshold for TRPM2 activation and revealed that the TRPM2 threshold is lowered by cytosolic Ca^{2+} . Importantly, PKC-mediated phosphorylation of TRPM2 appears to counteract the effect of cytosolic Ca^{2+} on TRPM2 thresholds, and may function as negative feedback signalling following cytosolic Ca^{2+} elevation caused by TRPM2 activation. The recent finding that the N-terminus of TRPM2 physically interacts with PKC γ to modify NMDA receptor functions (Zong et al., 2022) further supports our findings.

Despite the recent cryo-EM structural analysis revealing the tertiary structure of TRP channels, the detailed mechanism by which temperature increase activates thermo-TRPs remains largely unknown, in part because of the technical limitations associated with cryo-EM that do not allow visualisation of dynamic structural changes. The results of the present study show that phosphorylation of a single amino acid residue (T738) could regulate the temperature threshold for TRPM2 activation. This finding provides valuable structure-based clues for exploring the detailed mechanisms that determine and regulate the temperature threshold for TRPM2 activation.

References

- Bertil, H. (2001). *Ion channels in excitable membrane*. Sinauer.
- Boukalova, S., Marsakova, L., Teisinger, J., & Vlachova, V. (2010). Conserved residues within the putative S4-S5 region serve distinct functions among thermosensitive vanilloid transient receptor potential (TRPV) channels. *Journal of Biological Chemistry*, **285**(53), 41455–41462.

- Caterina, M. J., Schumacher, M. A., Tominaga, M., Rosen, T.A., Levine, J. D., & Julius, D. (1997). The capsaicin receptor: A heat-activated ion channel in the pain pathway. *Nature*, **389**(6653), 816–824.
- Csanady, L., & Torocsik, B. (2009). Four Ca²⁺ ions activate TRPM2 channels by binding in deep crevices near the pore but intracellularly of the gate. *Journal of General Physiology*, **133**(2), 189–203.
- Huang, Y., Roth, B., Lu, W., & Du, J. (2019). Ligand recognition and gating mechanism through three ligand-binding sites of human TRPM2 channel. *Elife*, **8**, e50175.
- Huang, Y., Winkler, P. A., Sun, W., Lu, W., & Du, J. (2018). Architecture of the TRPM2 channel and its activation mechanism by ADP-ribose and calcium. *Nature*, **562**(7725), 145–149.
- Kamm, G. B., Boffi, J. C., Zuza, K., Nencini, S., Campos, J., Schrenk-Siemens, K., Sonntag, I., Kabaoglu, B., El Hay, M. Y. A., Schwarz, Y., Tappe-Theodor, A., Bruns, D., Acuna, C., Kuner, T., & Siemens, J. (2021). A synaptic temperature sensor for body cooling. *Neuron*, **109**(20), 3283–3297.e11.
- Kashio, M., Sokabe, T., Shintaku, K., Uematsu, T., Fukuta, N., Kobayashi, N., Mori, Y., & Tominaga, M. (2012). Redox signal-mediated sensitization of transient receptor potential melastatin 2 (TRPM2) to temperature affects macrophage functions. *PNAS*, **109**(17), 6745–6750.
- Kashio, M., & Tominaga, M. (2017). The TRPM2 channel: A thermo-sensitive metabolic sensor. *Channels (Austin)*, **11**(5), 426–433.
- Kashio, M., & Tominaga, M. (2022). TRP channels in thermosensation. *Current Opinion in Neurobiology*, **75**, 102591.
- Luo, Y., Yu, X., Ma, C., Luo, J., & Yang, W. (2018). Identification of a Novel EF-Loop in the N-terminus of TRPM2 channel involved in calcium sensitivity. *Frontiers in Pharmacology*, **9**, 581.
- McHugh, D., Flemming, R., Xu, S. Z., Perraud, A. L., & Beech, D. J. (2003). Critical intracellular Ca²⁺ dependence of transient receptor potential melastatin 2 (TRPM2) cation channel activation. *Journal of Biological Chemistry*, **278**(13), 11002–11006.
- McKemy, D. D., Neuhauser, W. M., & Julius, D. (2002). Identification of a cold receptor reveals a general role for TRP channels in thermosensation. *Nature*, **416**(6876), 52–58.
- Moriyama, T., Higashi, T., Togashi, K., Iida, T., Segi, E., Sugimoto, Y., Tominaga, T., Narumiya, S., & Tominaga, M. (2005). Sensitization of TRPV1 by EP1 and IP reveals peripheral nociceptive mechanism of prostaglandins. *Molecular Pain*, **1**, 1744–8069-1-3.
- Numazaki, M., Tominaga, T., Toyooka, H., & Tominaga, M. (2002). Direct phosphorylation of capsaicin receptor VR1 by protein kinase Cε and identification of two target serine residues. *Journal of Biological Chemistry*, **277**(16), 13375–13378.
- Ramsey, I. S., Delling, M., & Clapham, D. E. (2006). An introduction to TRP channels. *Annual Review of Physiology*, **68**(1), 619–647.
- Rathee, P. K., Distler, C., Obreja, O., Neuhuber, W., Wang, G. K., Wang, S. Y., Nau, C., & Kress, M. (2002). PKA/AKAP/VR-1 module: A common link of Gs-mediated signaling to thermal hyperalgesia. *Journal of Neuroscience*, **22**(11), 4740–4745.
- Song, K., Wang, H., Kamm, G. B., Pohle, J., Reis, F. C., Heppenstall, P., Wende, H., & Siemens, J. (2016). The TRPM2 channel is a hypothalamic heat sensor that limits fever and can drive hypothermia. *Science*, **353**(6306), 1393–1398.
- Starkus, J., Beck, A., Fleig, A., & Penner, R. (2007). Regulation of TRPM2 by extra- and intracellular calcium. *Journal of General Physiology*, **130**(4), 427–440.
- Sumoza-Toledo, A., & Penner, R. (2011). TRPM2: A multifunctional ion channel for calcium signalling. *The Journal of Physiology*, **589**(7), 1515–1525.
- Tan, C. L., Cooke, E. K., Leib, D. E., Lin, Y. C., Daly, G. E., Zimmerman, C. A., & Knight, Z. A. (2016). Warm-sensitive neurons that control body temperature. *Cell*, **167**(1), 47–59.e15.
- Togashi, K., Hara, Y., Tominaga, T., Higashi, T., Konishi, Y., Mori, Y., & Tominaga, M. (2006). TRPM2 activation by cyclic ADP-ribose at body temperature is involved in insulin secretion. *Embo Journal*, **25**(9), 1804–1815.
- Tominaga, M., Caterina, M. J., Malmberg, A. B., Rosen, T. A., Gilbert, H., Skinner, K., Raumann, B. E., Basbaum, A. I., & Julius, D. (1998). The cloned capsaicin receptor integrates multiple pain-producing stimuli. *Neuron*, **21**(3), 531–543.
- Tong, Q., Zhang, W., Conrad, K., Mostoller, K., Cheung, J. Y., Peterson, B. Z., & Miller, B. A. (2006). Regulation of the transient receptor potential channel TRPM2 by the Ca²⁺-sensor calmodulin. *The Journal of Biological Chemistry*, **281**(14), 9076–9085.
- Uchida, K., Dezaki, K., Damdindorj, B., Inada, H., Shiuchi, T., Mori, Y., Yada, T., Minokoshi, Y., & Tominaga, M. (2011). Lack of TRPM2 impaired insulin secretion and glucose metabolisms in mice. *Diabetes*, **60**(1), 119–126.
- Vellani, V., Mapplebeck, S., Moriondo, A., Davis, J. B., & McNaughton, P. A. (2001). Protein kinase C activation potentiates gating of the vanilloid receptor VR1 by capsaicin, protons, heat and anandamide. *Journal of Physiology*, **534**(3), 813–825.
- Wang, L., Fu, T. M., Zhou, Y., Xia, S., Greka, A., & Wu, H. (2018). Structures and gating mechanism of human TRPM2. *Science*, **362**(6421), eaav4809.
- Wehrhahn, J., Kraft, R., Harteneck, C., & Hauschildt, S. (2010). Transient receptor potential melastatin 2 is required for lipopolysaccharide-induced cytokine production in human monocytes. *Journal of Immunology*, **184**(5), 2386–2393.
- Zong, P., Feng, J., Yue, Z., Li, Y., Wu, G., Sun, B., He, Y., Miller, B., Yu, A. S., Su, Z., Xie, J., Mori, Y., Hao, B., & Yue, L. (2022). Functional coupling of TRPM2 and extrasynaptic NMDARs exacerbates excitotoxicity in ischemic brain injury. *Neuron*, **110**(12), 1944–1958.e8.

Additional information

Data availability statement

All data that support the findings of the present study are provided in the published paper.

Competing interests

The authors declare that they have no competing interests.

Author contributions

MK designed the study, performed the experiments and analysed the data. MK, SM and MT wrote the manuscript. All authors have read and approved the final version of the submitted manuscript for publication and agree to be accountable for all aspects of the work in ensuring that questions related to the accuracy or integrity of any part of the work are appropriately investigated and resolved. All persons designated as authors qualify for authorship, and all those who qualify for authorship are listed.

Funding

This work was supported by grants from a Grant-in Aid for Scientific Research from the Ministry of Education, Culture, Sports, Science and Technology in Japan (#20K06748 for

MK; #21H02667 and #20H05768 for MT), the 24th General Assembly of the Japanese Association of Medical Sciences (MK) and the Takeda Science Foundation (MK).

Acknowledgements

We thank Dr Takaaki Sokabe for helpful advice. We also thank N. Fukuta and C. Saito for their technical assistance.

Keywords

calcium, phosphorylation, temperature threshold, TRPM2

Supporting information

Additional supporting information can be found online in the Supporting Information section at the end of the HTML view of the article. Supporting information files available:

Statistical Summary Document

Peer Review History